Aggressive Cholesterol Lowering Normalizes Atherosclerosis Regression in *Jak2*^{V617F} Clonal Hematopoiesis

Brian D. Hardaway (MPhil)[1], Trevor P. Fidler (PhD)[2], Mojdeh Tavallaie (PharmD-PhD)[1], Kleopatra Avrampou (PhD)[1], Cheng-Chieh Hsu (PhD)[1], Sandra Schiavone (MA)[1], Tong Xiao (MS)[1], Nan Wang (PhD)[1*], Alan R. Tall (MD)[1*]

[1]Division of Molecular Medicine, Department of Medicine, Columbia University Irving Medical Center, New York, NY, USA.

[2]Cardiovascular Research Institute, University of San Francisco, San Francisco, CA, USA.

Short Title: Atherosclerosis Regression in *Jak2*^{V617F} CH

[*]These authors contributed equally to this work.

Correspondence to:

Alan R. Tall: art1@cumc.columbia.edu

Abstract

Background - Clonal hematopoiesis (CH) has emerged as an important risk factor for atherosclerotic cardiovascular disease (ACVD). Mouse studies have established a causal role of CH in atherosclerosis progression and have defined macrophage inflammatory responses as a key underlying mechanism. We undertook the present study to assess the hypothesis that ongoing inflammation would impede atherosclerosis regression in *Jak2*^{V617F} (*Jak2*^{VF}) CH mice.

Methods and Results - Chimeric *Jak2*$^{VF/WT}$ or control *WT/WT* bone marrow was transplanted into *Ldlr*$^{-/-}$ mice and, following 13-16 weeks of Western diet-induced atherosclerosis progression, cholesterol was lowered either moderately (to 200-300 mg/dl) or markedly (to 100 mg/dl). With moderate cholesterol lowering there was impaired regression in *Jak2*^{VF} CH mice compared to controls. However, with marked cholesterol lowering, regression was similar in *Jak2*^{VF} CH and control mice.

Two mechanisms of low-density lipoprotein (LDL) lowering-induced suppression of inflammation in plaques were implicated: 1) reversal of increased proliferation, DNA damage and Absent in Melanoma 2 (AIM2) inflammasome activation specifically in *Jak2*^{VF} macrophages and 2) markedly increased macrophage triggering receptor expressed on myeloid cells 2 (TREM2), c-myc expressing macrophages in both *Jak2*^{VF} and control mice.

Conclusions - Aggressive LDL lowering reverses inflammasome activation and induces pro-resolving changes in macrophages in *Jak2*^{VF} CH, halting atherosclerosis progression and promoting features of plaque stabilization. These findings suggest that aggressive LDL cholesterol lowering could effectively reverse ACVD risk in individuals with *JAK2*^{VF} clonal hematopoiesis.

35 **Translational Perspective**

36 Clonal hematopoiesis increases the risk of atherosclerotic cardiovascular disease. Amongst
37 mutations associated with clonal hematopoiesis, *Jak2*^{V617F} confers the greatest increased risk of
38 atherosclerotic cardiovascular disease. Our findings demonstrate that aggressive LDL lowering
39 normalizes atherosclerosis regression in *Jak2*^{V617F} clonal hematopoiesis by reversing
40 inflammasome activation and inducing pro-resolving changes in macrophages. These changes
41 lead to increased features of plaque stability, including decreased macrophage burden, increased
42 collagen, and improved efferocytosis. These results suggest that aggressive LDL-C lowering in
43 *Jak2*^{V617F} clonal hematopoiesis patients would mitigate the increased atherosclerotic
44 cardiovascular disease risk.

45 **1. Introduction**

46 Despite therapeutic advances, ACVD remains the leading cause of death in the developed
47 world.[1] Although inflammation plays a key role in atherosclerosis progression, cholesterol
48 accumulation remains a prerequisite for lesion development, and LDL lowering has consistently
49 shown a benefit in many clinical trials.[2-4]

50 The role of inflammation in increasing ACVD risk has also now been well established. The
51 LoDoCo 2 trial found that the risk of cardiovascular events was significantly lower in patients
52 with chronic coronary disease who were given 0.5 mg of colchicine daily.[5] Based on these and
53 other results, the FDA approved the use of low dose colchicine as the first anti-inflammatory
54 drug for heart disease.[6] The CANTOS trial involving the use of interleukin-1β (IL-1β) antibodies
55 showed reduced cardiovascular events in high-risk patients with mean LDL cholesterol levels of
56 81 mg/dl - 84 mg/dl and a high-sensitivity C-reactive protein (hs-CRP) level of at least 2 mg/L.

57 However, there was a small increase in fatal infections, and the FDA did not approve this
58 treatment for marketing.[7] Many observations suggest that hypercholesterolemia is linked to
59 inflammatory risk. For example, statins lower hs-CRP levels[8] and preclinical studies have shown
60 that cholesterol accumulation in plaque macrophages promotes inflammasome activation.[9-12]
61 However, the mechanisms linking hypercholesterolemia, macrophage cholesterol accumulation
62 and inflammation remain incompletely understood, especially in the clinically important context
63 of atherosclerosis regression induced by LDL lowering.[13-19]

64 Clonal hematopoiesis (CH) arises from somatic mutations in hematopoietic stem cells (HSC) that
65 confer a selective advantage and lead to clonal expansion of blood cells. CH commonly arises
66 from mutations in genes that mediate epigenetic modifications or cytokine signaling.[20,21]
67 Amongst CH mutations, *Jak2*^{VF}, which increases signaling by hematopoietic cytokines, confers
68 the greatest risk of ACVD.[22-24] Moreover, *JAK2*^{VF} has been detected in 3-4% of a general
69 European population,[25] and increases thrombotic risk and coronary artery plaque erosion even at
70 low variable allele frequency().[26,27,28] We showed in a hypercholesterolemic mouse model that
71 *Jak2*^{VF} CH exacerbates atherosclerosis via AIM2 inflammasome activation in mice[29] with genetic
72 studies suggesting a similar role in humans.[30] The AIM2 inflammasome is activated by double
73 stranded DNA fragments in the cytosol.[31] We proposed two potential mechanisms of DNA
74 damage underlying AIM2 inflammasome activation in *Jak2*^{VF} CH: increased proliferation of
75 *Jak2*^{VF} macrophages leading to DNA replication stress or increased mitochondrial glycolytic
76 metabolism, reactive oxygen species (ROS) formation and oxidative DNA damage. Based on
77 these findings, we hypothesized that LDL lowering-induced atherosclerosis regression would be
78 impaired in *Jak2*^{VF} CH mice due to persistence of the underlying mechanisms promoting
79 inflammasome activation. Contrary to our hypothesis, we found that cholesterol lowering

80 reversed inflammasome associated changes in *Jak2*^{VF} macrophages and that marked cholesterol
81 lowering induced regression similar to control mice. These studies suggest the importance of
82 rigorous control of LDL cholesterol levels in individuals with *JAK2*^{VF} clonal hematopoiesis.

83 **2. Methods**

84 Several experimental procedures were performed as previously described[16,29]

85 **2.1 Mice**

86 All mice used for these studies were male and on a C57BL/6J background. Mice were housed in
87 a pathogen-free facility under standard conditions of temperature (23 °C) with a 12-hour light-
88 dark with ad libitum food and water access. Cages and water were changed every 7-14 days. All
89 mouse experiments were approved by the Institutional Animal Care and Use Committee of
90 Columbia University under protocol number AABG0561, and were conducted in accordance
91 with NIH guidelines and the Guide for the Care and Use of Laboratory Animals. Mice
92 heterozygous for the *Jak2*^{VF} conditional knock-in allele were generated as previously
93 described.[32] *Jak2*^{VF} mice were then crossed to *Mx1-Cre* (The Jackson Laboratory, B6.Cg-
94 Tg(*Mx1-Cre*)1*Cgn*/J (003556) or *Scl-Cre* (The Jackson Laboratory, C57BL/6-Tg(Tal1-
95 cre/ERT)42-056Jrg/J (037466) to generate *Mx1-CreJak2*^{VF} and *Scl-CreJak2*^{VF} mice respectively.
96 *Scl-Cre-Jak2*^{VF} mice were then crossed with ZsGreen reporter mice (The Jackson Laboratory,
97 B6.Cg-Gt(ROSA)26Sor$^{tm6(CAG-ZsGreen1)Hze}$/J (Ai6(RCL-ZsGreen) (007906) to generate *Scl-*
98 *CreJak2*^{VF}*ZsGreen* mice. *Ldlr*$^{-/-}$ recipient mice for the *Mx1-CreJak2*^{VF} moderate cholesterol
99 lowering model that included *Myh11-Cre*^{ERT2} and *ZsGreen* alleles from a previous lineage-tracing
100 study were obtained from a collaborator and have been previously described.[33] However, these
101 alleles were not relevant to the experimental outcomes assessed and were not analyzed. Half of

102 the recipients were *Ldlr*$^{-/-}$ *Myh-11-CreZsGreen* while the other half either lacked the *ZsGreen*
103 allele or both the *ZsGreen* allele and the *Myh11-Cre*. For the *Mx1-CreJak2*^{VF} and *Scl-CreJak2*^{VF}
104 aggressive cholesterol lowering studies, *Ldlr*$^{-/-}$ recipient mice were purchased from The Jackson
105 Laboratory (B6.129S7-*Ldlr*tm1Her/J (002207)). Littermate control mice for studies involving
106 *Mx1-CreJak2*^{VF} mice contained either an allele with *Mx1-Cre* or the *Jak2*^{VF} transgene, but not
107 both. Littermate control mice for studies involving *Scl-CreJak2*^{VF}*ZsGreen* mice contained the
108 alleles for *Scl-Cre* and *ZsGreen* but not the *Jak2*^{VF} transgene.

109 **2.2 Bone Marrow Transplantation**

110 Bone marrow transplantations (BMT) were conducted as previously described with the following
111 exceptions.[10] For the *Mx1-CreJak2*^{VF} moderate cholesterol lowering study, donor mice were 8-12
112 weeks old while recipients were 11-14 weeks old. For the *Mx1-CreJak2*^{VF} effective cholesterol
113 lowering study, donor mice were 7-16 weeks old while recipients were 7 weeks old. For the *Scl-*
114 *CreJak2*^{VF} study, donor mice were 6-12 weeks old while recipients were 8 weeks old. For the
115 *Mx1-CreJak2*^{VF} moderate cholesterol lowering study, recipients were lethally irradiated once
116 with 10.5 Gy from a cesium gamma source. Due to decommissioning of the cesium gamma
117 source, recipients from the *Mx1-CreJak2*^{VF} and *Scl-CreJak2*^{VF} effective cholesterol lowering
118 studies were irradiated with 10.5 Gy using a Multirad 350 X-ray Irradiator from Precision X-
119 Ray. Within 24 hours of irradiation, bone marrow was isolated from donors with the indicated
120 genotypes. Total bone marrow cell number was quantified using an iN CYTO C-Chip
121 hemocytometer (DHC-N01) according to the manufacturer instructions. Irradiated mice were
122 randomized to treatment groups, anesthetized with isoflurane before receiving 3 x 10^6 total bone
123 marrow cells via intravenous (i.v.) injection at a total final volume of 100 µl. For the *Mx1-*
124 *CreJak2*^{VF} studies, recipients received either 6 x 10^5 *CD45.1Mx1-CreJak2*$^{VF/WT}$ or 6 x 10^5

125 *CD45.1* control bone marrow cells (20%) combined with 2.4 x 10^6 *CD45.2Jak2*$^{WT/WT}$ cells (80%).
126 For the *Scl-CreJak2*^{VF} study, recipients received either 6 x 10^5 *CD45.1CD45.2Scl-*
127 *CreJak2*$^{VF/WT}$*ZsGreen* or 6 x 10^5 *CD45.1CD45.2Scl-CreJak2*$^{WT/WT}$*ZsGreen* bone marrow cells
128 (20%) combined with 2.4 x 10^6 *CD45.1Jak2*$^{WT/WT}$ cells (80%). For the *Mx1-CreJak2*^{VF} studies,
129 mice were allowed to recover for four weeks after BMT before being injected intraperitonially
130 (i.p.) with 50 µg/mouse/day polyinosinic:polycytidylic acid (pIpC) two times, 48 hours apart.

131 **2.3 Atherosclerosis Studies**

132 For the *Mx1-CreJak2*^{VF} studies, power analysis using GPower3.1 indicated that with a total
133 sample size of 80 (n = 20 per group), the study had 80% power to detect an effect size of f = 0.32
134 at $\alpha = 0.05$, using two-way analysis of variance (ANOVA) across two genotypes and two
135 treatments. For the *Scl-CreJak2*^{VF} study, power analysis using GPower3.1 indicated that with a
136 total sample size of 80 (n = 16 per group), the study had 80% power to detect an effect size of f =
137 0.40 at $\alpha = 0.05$, using one-way ANOVA across five groups. Four weeks after BMT. *Ldlr*$^{-/-}$
138 recipient mice were fed a western diet (ENVIGO, cat. no. TD.88137) for the indicated times. For
139 the final 10 days of the western diet period of the *Scl-CreJak2*^{VF} study, mice were switched to a
140 western diet containing tamoxifen at 500 mg/kg by weight (ENVIGO, cat. no. TD130889). To
141 induce LDL lowering in the *Mx1-CreJak2*^{VF} study of Figure 1A, mice were administered 2 x 10^{11}
142 viral particles per mouse in 200 µl of 1X PBS via tail vein injection of an hDAD-*hLDLr* viral
143 vector (Gene Vector Core Laboratory at the Baylor College of Medicine) and switched to chow
144 diet. To induce LDL lowering in the *Mx1-CreJak2*^{VF} study of Figure 4A and the *Scl-CreJak2*^{VF}
145 study of Figure 6A, mice were administered 2.5 x 10^{11} genome copies per mouse in 100 µl of 1X
146 PBS via tail vein injection of an AAV8-TBG-*mLdlr* vector (AAV-263355, Vector Biolabs) and
147 switched to chow diet. Mice were anesthetized using 5% isoflurane via inhalation at a flow rate

148 of approximately 3L/min oxygen using a calibrated vaporizer. Anesthetic depth was assessed
149 continuously using respiratory rate monitoring and the toe-pinch reflex. Isoflurane was
150 administered acutely during procedures requiring anesthesia, including blood collection and
151 euthanasia. Blood collection was performed via retro-orbital sinus for plasma, complete blood
152 counts, and flow cytometric analysis at the indicated timepoints. For euthanasia, mice were first
153 rendered deeply unconscious with isoflurane, after which cervical dislocation was performed as a
154 secondary method to ensure death, in accordance with AVMA guidelines. Following euthanasia,
155 aortic roots were collected and fixed with 4% paraformaldehyde (PFA) (Electron Microscopy
156 Sciences 15710; 16% PFA diluted 1:4 in 1.33X PBS) for 24 hours at 4 $^{\circ}$C , then embedded in
157 paraffin.

158 **2.4 Histological Analysis**

159 Lesion area and necrotic core area were quantified as previously described.[22,29] Researchers
160 blinded to genotype sectioned paraffin-embedded aortic root lesions at similar points between
161 mice over a 150 µm span for a total of 50 sections spaced 3 µm apart with 2 sections per slide on
162 25 slides. Six total slides spaced 30 µm apart (slides 1,5,10,15,20,25) were then stained with
163 hematoxylin & eosin (H&E) (Sigma MHS32-1L; Abcam ab246824) and imaged with an
164 Olympus DP27 camera attached to an Olympus CX43 biological microscope set to the 10X
165 objective using Olympus cellSens Entry 3.1 software. Lesion area was then quantified in a
166 blinded fashion and the average of the six slides was used to determine lesion area. The Necrotic
167 core area was similarly quantified in a blinded fashion using the same six H&E sections.
168 Collagen was stained using the Polysciences Picrosirius Red Stain Kit (cat. no. 24901) according
169 to the manufacturer's instructions. The same slide between mice was stained and the collagen
170 quantified by applying a consistent color threshold to calculate the collagen-positive area as a

171 percentage of total lesion area. Picrosirius red was imaged via the same system used for H&E
172 imaging. All lesion analysis was conducted using FIJI software.

173 **2.5 Immunofluorescence**

174 Identical slides of aortic roots between mice were baked in a dry incubator at 60 °C for 30
175 minutes and then deparaffinized in Histo-clear (National Diagnostics HS-200/50-899-90147)
176 three times for 10 minutes. Histo-clear was removed by 20 shakes in 100% ethanol twice
177 followed by 20 shakes in Histoprep Reagent Alcohol (fisher HC-600-1GAL) before being
178 washed in tap water 7 times. Antigen retrieval was performed by placing slides either in citric
179 acid-based antigen retrieval solution (Vector Laboratories, H3300) or tris-based antigen retrieval
180 solution (Vector Laboratories, H3301) and pressure cooking for 15 minutes with a 5-minute
181 natural release in an Instant Pot IP-LUX pressure cooker. Citric acid-based antigen retrieval was
182 performed for all antibodies except for the antibody against cleaved GasD. After pressure
183 cooking, slides were cooled for 10 minutes and then washed 3 times for 5 minutes in 1X
184 phosphate buffered saline (PBS) (Boston Bioproducts BM-220; diluted 1:10). Hydrophobic
185 circles were drawn using a liquid blocker pen (Sigma Z377821). For antibodies sourced from
186 mice, mouse on mouse blocking was performed by incubating sections in 10% goat serum
187 (ThermoFisher 10000C) in 1X PBS (Corning 21-040-CM) with 1 drop of mouse-on-mouse block
188 per 1.25ml of solution (Vector Laboratories NC9290646) for 1 hour at room temperature in a
189 humidified chamber. Slides were then washed in 1X PBS containing tween 20 (Fisher BP337-
190 500) at a concentration of 0.01% (PBS-T) twice for 5 minutes and then in 1X PBS once for 5
191 minutes. For antibodies not sourced from mice, sections were blocked by incubating in Normal
192 Serum Block (Biolegend 927503) for 1 hour at room temperature in a humidified chamber.
193 Following blocking, sections were incubated with the following primary antibodies at the

194 indicated dilutions or concentrations overnight at 4 °C in a humidified chamber: AIM2 (Abcam,
195 ab119791, 1:250), 8-hydroxydeoxyGuanosine (Abcam, ab183395, 1:100), Cleaved GasD (Cell
196 Signaling, 10137, 10µg/ml), c-myc (Cell Signaling, 5605, 5.76 µg/ml), Ki67 (Abcam, ab15580,
197 9 µg/ml), MAC2 conjugated to Alexa Fluor 488 (Cedarlane, CL8942AF4, 1 µg/ml), MAC2
198 (Cedarlane, CL8942AP, 1 µg/ml), MerTK (R&D, BAF591, 2 µg/ml), pγH2AX (Cell Signaling,
199 9718, 0.74 µg/ml), ZsGreen (ThermoFisher, TA180002, 10 µg/ml), TREM2 (Denali, 4D9
200 DC1847, 1:100). The following IgG antibodies were used as negative controls for primary
201 antibodies sourced from the same species at the same concentration: Mouse IgG (ChromPure,
202 015-000-003), Rabbit IgG (Abcam, ab172730), Rabbit IgG (Novus Biologicals, NBP2-24891),
203 Rabbit IgG (ChromPure 011-000-003), Rat IgG (ChromPure, 012-000-003), Rat IgG (Biolegend,
204 400431), Rat IgG conjugated to Alexa Fluor 488 (Invitrogen, 53-4321-80). Slides were then
205 washed twice with PBS-T for 5 minutes and once with 1X PBS for 5 minutes. The following
206 secondary antibodies were used at a dilution of 1:200 for 1 hour at room temperature: Rat
207 conjugated to Alexa Fluor 488 (Invitrogen A11006), Rat conjugated to Alexa Fluor 568
208 (Invitrogen A11077), Rat conjugated to Alexa Fluor 647 (Invitrogen A-21247), Rabbit
209 conjugated to Alexa Fluor 568 (Invitrogen A11011), Rabbit conjugated to Alexa Fluor 647
210 (A27040). The following secondary antibodies were used at a dilution of 1:800 for 1 hour at
211 room temperature: Mouse conjugated to Alexa Fluor 647 (Invitrogen A21237), Streptavidin
212 conjugated to Alexa Fluor 568 (Invitrogen S11226), Streptavidin conjugated to Alexa Fluor 647
213 (Invitrogen S32357). DAPI (4',6-Diamidino-2-Phenylindole, Dilactate) (Biolegend, 422801) was
214 included during incubation with secondary antibodies at a concentration of 5 µg/ml. Slides were
215 then washed twice with PBS-T for 5 minutes and once with 1X PBS for 5 minutes. After
216 washing, slides were mounted using Prolong Gold Antifade Reagent with DAPI (Invitrogen

217 P36935). TUNEL staining was performed using the In Situ Cell Death Detection Kit TMR Red
218 (Roche, 12156792910) according to the manufacturer's instructions. Slides were imaged on a
219 Leica Fluorescent DMI 6000B wide-field microscope or a Nikon Ti Eclipse inverted microscope
220 with high-sensitivity confocal imaging at the Confocal and Specialized Microscopy Shared
221 Resource (CSMSR) Core at Columbia University. All images were analyzed in a blinded fashion
222 using FIJI software.

223 **2.6 Statistics**

224 Statistical analyses were conducted using GraphPad Prism v10.5. Data are presented as the mean
225 ± s.e.m., with all measurements obtained from distinct biological samples. All statistical tests
226 were performed using two-sided analyses. Normality was tested using the D'Agostino-Pearson
227 omnibus and, where appropriate, log transformation was applied to approximate normality.
228 Formal outliers were removed using a two-tailed Grubbs' test ($\alpha = 0.05$). Repeated measures data
229 were analyzed using two-way ANOVA with the Geisser-Greenhouse correction for sphericity and
230 Tukey's multiple comparisons test with individual variance estimation. For datasets involving
231 two independent variables, two-way ANOVA with Tukey's multiple comparisons test or Kruskal-
232 Wallis with Dunn's multiple comparisons test were used based on distribution. For datasets
233 involving five experimental groups, one-way ANOVA with Holm-Sidak's multiple comparisons
234 test or Kruskal-Wallis with Dunn's multiple comparisons test were used based on distribution.

235 Details of blood analysis can be found in the supplement.

236 **3. Results**

237 **3.1 Atherosclerosis Regression is Impaired with Moderate Cholesterol Lowering in *Jak2*^{VF}**
238 **CH**

239 To assess the effect of *Jak2*^{VF} CH on atherosclerosis regression, we placed *Jak2*^{VF} CH male mice
240 and controls on a western diet for 16 weeks and then induced cholesterol lowering using a
241 Helper-dependent Adenoviral vector containing the human LDL receptor gene (hDAD-hLDLR)
242 combined with a switch to chow diet for an additional 5 weeks (Figure 1A). Prior studies were
243 performed in female mice.[16,29] *Jak2*^{VF} CH male mice exhibited splenomegaly, lower body
244 weight, and increased RBCs, hematocrit, red blood cell distribution width (RDWc), and
245 neutrophils, mirroring previous findings in females (Supplemental Figure 1A-I).[29] In this model,
246 CD45.1+ cells are *Jak2*^{VF} in experimental mice and WT in controls. CD45.1+ neutrophils and
247 monocytes were elevated while CD45.1+ lymphocytes were reduced (Supplemental Figure 1J-
248 L). Plasma cholesterol was reduced in *Jak2*^{VF} CH mice on western diet (Figure 1B) similar to
249 previous findings in female mice and humans.[24,29,34] Plasma cholesterol remained moderately
250 elevated 10 days post-virus treatment but returned to pre-diet levels (~200-300 mg/dl) by the end
251 of the regression period (Figure 1B). At baseline, lesion area and necrotic core area were
252 significantly increased in the aortic root of male *Jak2*^{VF} CH mice compared to controls,
253 confirming that *Jak2*^{VF} CH worsens atherosclerosis in both male and female mice (Figure 1C-
254 E).[29] Moderate cholesterol lowering halted progression of lesion and necrotic core area in control
255 mice whereas *Jak2*^{VF} CH mice developed significantly larger necrotic cores and displayed a
256 strong trend toward increased lesion area (p=0.052) (Figure 1C-E). Consistent with previous
257 regression studies,[35,36] lesional collagen was increased in control mice after cholesterol lowering
258 with no significant change in *Jak2*^{VF} CH mice, further indicating impaired regression in the
259 *Jak2*^{VF} CH mice (Figure 1F,G). The most consistent phenotype found in atherosclerosis
260 regression studies has been a decrease in macrophage burden.[13,17-19,36] Macrophages were
261 significantly decreased in control mice but not in *Jak2*^{VF} CH mice after cholesterol lowering

262 (Figure 1H,I). These results indicate that atherosclerosis regression is impaired in *Jak2*^{VF} CH
263 with moderate cholesterol lowering.

264 We next assessed whether impaired regression in *Jak2*^{VF} CH mice was associated with persistent
265 inflammatory features in plaques. Necrotic, inflammatory cell death is mediated by activated
266 Gasdermin D (GasD) downstream of inflammasome activation.[37] We used an antibody to the
267 active N-terminal fragment of GasD to assess pyroptosis in plaques.[38] Total cleaved GasD in
268 plaques as well as cleaved GasD in the necrotic core were increased in *Jak2*^{VF} CH lesions at
269 baseline and were not reduced by cholesterol lowering (Figure 2A-C). However, macrophage-
270 specific cleaved GasD was decreased by cholesterol lowering in *Jak2*^{VF} CH lesions, suggesting
271 that macrophage pyroptosis had been suppressed by the time of harvest (Figure 2D,E).
272 Consistent with earlier findings in females, AIM2+ macrophages and phosphorylated histone
273 H2A.X (pγH2AX), an indicator of double stranded DNA break formation, were increased in
274 *Jak2*^{VF} CH lesions at baseline and were decreased by cholesterol lowering, suggesting reversal of
275 AIM2 inflammasome activation (Figure 2F-I).[29] Additionally, macrophage proliferation trended
276 higher at baseline in *Jak2*^{VF} CH mice and was significantly reduced by cholesterol lowering
277 (Figure 2J,K). Macrophage oxidized DNA was increased in control lesions and unchanged by
278 cholesterol lowering in *Jak2*^{VF} CH lesions (Figure 2L,M). These data suggest reversal of
279 macrophage AIM2 inflammasome activation and pyroptosis by moderate cholesterol lowering in
280 *Jak2*^{VF} CH mice, correlating with decreased macrophage proliferation and decreased DNA
281 damage response but not with oxidative DNA damage changes. The persistence of cleaved GasD
282 in the necrotic core area may reflect ongoing pyroptosis during the early phase of regression
283 when cholesterol levels were persistently elevated and could explain impaired regression in the
284 *Jak2*^{VF} mice.

285 **3.2 Cholesterol Lowering Restores Impaired Efferocytosis and increases TREM2+**
286 **Macrophages in *Jak2*^{VF} CH Lesions**

287 Atherosclerosis regression has been associated with improvements in pro-resolving features such
288 as increased macrophage efferocytosis, mer proto-oncogene tyrosine kinase (MerTK)
289 expression,[13,39,40] increased numbers of TREM2+ macrophages and limitation of necrotic core
290 formation in plaques.[16,41] During atherosclerosis progression, macrophage MerTK and TREM2
291 were suppressed in *Jak2*^{VF} CH mouse plaques as a result of interleukin-1 (IL-1) signaling from
292 mutant to wild-type (WT) cells.[38] Consistent with these studies, we found that macrophage
293 MerTK was decreased in *Jak2*^{VF} CH lesions at baseline compared to controls (Figure 3A,B).
294 MerTK levels were completely restored by cholesterol lowering (Figure 3A,B). Additionally, we
295 found that cholesterol lowering dramatically increased the percentage of macrophages positive
296 for TREM2 in both control and *Jak2*^{VF} CH lesions (Figure 3C,D). Consistent with these findings,
297 macrophage-associated TUNEL+ nuclei as a percentage of total lesional TUNEL+ nuclei, an
298 estimate of in situ efferocytosis,[14] were significantly decreased in *Jak2*^{VF} CH lesions at baseline
299 and restored by cholesterol lowering, (Figure 3E,F). Together, these data suggest that cholesterol
300 lowering restores impaired efferocytosis in *Jak2*^{VF} CH lesions and increases the proportion of
301 inflammation-resolving macrophages in lesions. Thus, macrophage inflammasome activation and
302 associated defects in efferocytosis were reversed by cholesterol lowering in *Jak2*^{VF} CH mice. The
303 increased necrotic core and decreased collagen content in these mice could reflect limited
304 resolution of hypercholesterolemia during the earlier phases of regression.

305 **3.3 More Effective Cholesterol Lowering Restores Atherosclerosis Regression**

306 To test this hypothesis, we performed a similar regression study but with more effective LDL
307 cholesterol lowering. Murine LDL does not bind as strongly to the human LDLR (employed in

308 Figure 1) as to the mouse LDLR.[42,43] Therefore, we employed an Adeno-Associated Virus
309 serotype 8 vector (AAV8) containing the mouse *Ldlr* gene which more effectively and more
310 quickly lowered cholesterol levels (Figure 4A). In this model, CD45.1+ cells are *Jak2*^{VF} in
311 experimental mice and WT in controls. Again, *Jak2*^{VF} CH mice exhibited splenomegaly, lower
312 body weight, and increased RBCs, hematocrit, and RDWc while CD45.1+ neutrophils and
313 monocytes were elevated, and these parameters were not appreciably changed by cholesterol
314 lowering (Supplemental Figure 2, Figure 4B). Consistent with the first study, lesion area and
315 necrotic core area were significantly increased in *Jak2*^{VF} CH mice at baseline. However, in
316 contrast to the first study, while both groups showed similar upwards trends, there was no
317 significant change in lesion area or necrotic core area in either group after aggressive LDL
318 lowering (Figure 4C-E). Furthermore, aggressive cholesterol lowering significantly increased
319 lesional collagen and decreased macrophage burden in both groups (Figure 4F-I). Analysis of
320 cleaved GasD showed an increase in macrophages in *Jak2*^{VF} mice at baseline that was reversed
321 by cholesterol lowering, and in contrast to the first study a decrease in cleaved GasD in the
322 necrotic core that appeared to involve both control and *Jak2*^{VF} CH mice (Supplemental Figure
323 3A-D). Consistent with the first study, double stranded DNA breaks (pγH2AX) were increased in
324 Jak2VF CH lesions at baseline and more strongly decreased by aggressive cholesterol lowering
325 along with a significant decrease in macrophage proliferation (Supplemental Figure 3E-H).
326 Additionally, macrophage MerTK was increased by aggressive cholesterol lowering in a manner
327 consistent with the first study (Supplemental Figure 3I,J). These results indicate that more
328 effective cholesterol lowering completely reversed inflammatory features and induced similar
329 levels of atherosclerosis regression in control and *Jak2*^{VF} CH lesions.

330 **3.4 Cholesterol Lowering Suppresses Proliferation of *Jak2^{VF}* Macrophages and increases c-**
331 **Myc+TREM2+ Macrophages**

332 The first two studies indicated that effective cholesterol lowering could reverse impaired
333 regression and the underlying cellular defects that promote AIM2 inflammasome activation.
334 However, in these studies *Jak2^{VF}* was active during progression and lesion area was increased at
335 baseline, potentially influencing the results. To simulate the situation where the *Jak2^{VF}* mutation
336 was acquired later in life after atherosclerosis had already developed, we performed a third study
337 in which *Jak2^{VF}* was activated in HSCs at the start of regression by using a tamoxifen-inducible
338 Scl-driven cre recombinase along with a floxed ZsGreen reporter allele (*Jak2^{VF} Scl* CH) to assess
339 cell genotype specific changes (Figure 5A). In addition to the two cholesterol lowering groups
340 (regression groups) we also included control and *Jak2^{VF}* mice that remained on the western diet
341 (progression groups). As expected, plasma cholesterol remained elevated in the progression
342 groups but was markedly and rapidly decreased in both regression groups (Figure 5B). In this
343 model, cells double positive for CD45.1 and CD45.2 are *Jak2^{VF}* in experimental mice and WT in
344 controls. The *Jak2^{VF}* phenotype was partially apparent as indicated by increased spleen weights,
345 RDWc, and hematocrit as well as expansion of CD45.1+CD45.2+ blood monocytes and
346 neutrophils, but less pronounced than in the earlier studies when *Jak2^{VF}* was activated prior to
347 Western diet feeding (Supplemental Figure 4).

348 Compared to the earlier models, the impact of *Jak2^{VF}* on lesion progression was less pronounced
349 which likely reflects the shorter period of *Jak2^{VF}* activation (Supplemental Figure 5A-C).
350 However, consistent with the earlier studies, the necrotic core significantly worsened in the
351 *Jak2^{VF} Scl* CH progression mice but not in the control *Scl* mice compared to baseline, while the
352 necrotic core was not significantly changed in either regression group compared to baseline

353 (Supplemental Figure 5C). Additionally, macrophage burden was similarly decreased in both
354 regression groups, (Supplemental Figure 5D,E). These studies further support that aggressive
355 cholesterol lowering similarly promotes regression in control and *Jak2*^{VF} CH mice, compared to
356 progression or baseline groups, in mice with *Jak2*^{VF} only activated at the beginning of the
357 regression period.

358 Cleaved GasD was increased in *Jak2*^{VF} CH lesions compared to baseline and trended lower
359 (p=.06) after cholesterol lowering, consistent with aggressive cholesterol lowering reversing
360 pyroptosis in lesions (Figure 5C,D). In the *Jak2*^{VF} CH progression group, proliferation was
361 significantly increased in *Jak2*^{VF} (green) macrophages but not in WT (non-green) macrophages
362 indicating a mutant cell specific effect, as seen previously.[29] Notably, this was reversed by
363 cholesterol lowering indicating that proliferation of the *Jak2*^{VF} cells was highly dependent on
364 LDL cholesterol levels (Figure 5E-G). Consistently, the DNA damage response (pγH2AX) was
365 significantly increased in *Jak2*^{VF} cells, and this was reversed by cholesterol lowering while WT
366 cells showed no significant changes within *Jak2*^{VF} CH lesions (Figure 5H-J). This suggests that
367 cell autonomous proliferation and associated formation of double stranded DNA breaks is
368 reversed by cholesterol lowering in lesions of *Jak2*^{VF} CH mice.

369 Given that a proliferative efferocytic population with high c-Myc expression has been described
370 during regression,[13,39] we assessed c-Myc expression along with TREM2. In contrast to the
371 decreases in Ki67, macrophage c-Myc and c-Myc+TREM2^{Hi} macrophages were increased
372 during regression in both control and *Jak2*^{VF} mice, suggesting a selective increase of TREM2+,
373 anti-inflammatory macrophages despite a decrease in total macrophages (Figure 6).

374 **4. Discussion**

375 We previously showed that the combination of LDL lowering and *Jak2*^{VF} genetic inactivation
376 induced fibrous cap thickening and increased TREM2^{Hi} macrophages in *Jak2*^{VF} CH mice.[16]
377 Given the propensity of plaque *Jak2*^{VF} mutant cells to proliferation, DNA damage, and AIM2
378 inflammasome activation,[29] we hypothesized that LDL lowering alone would be insufficient to
379 induce plaque regression in *Jak2*^{VF} mice. While this proved to be the case with moderate LDL
380 lowering, aggressive cholesterol lowering produced plaque regression (or halted progression)
381 similarly in controls and *Jak2*^{VF} CH mice. Surprisingly, LDL lowering reversed the major
382 cellular changes in *Jak2*^{VF} macrophages that have been associated with athero-progression. This
383 included reduced AIM2 expression and pyroptosis and increased MerTK, TREM2 and in situ
384 efferocytosis that have all been mechanistically linked in prior studies of *Jak2*^{VF} mice.[38] Whereas
385 we previously considered glycolytic mitochondrial ROS production and oxidative DNA damage
386 as a likely mechanism underlying AIM2 inflammasome activation, the reversal of pyroptosis by
387 cholesterol lowering was not associated with reduced oxidized DNA. Rather, decreased
388 macrophage proliferation and reduced replication stress appears to be the major mechanism
389 underlying reversal of pyroptosis.

390 Studies of atherosclerosis regression induced by LDL lowering in mouse models have revealed
391 multiple underlying mechanisms[44] including macrophage emigration,[45] decreased monocyte
392 entry[46] and a key role of acquired immunity and T-regs.[17] Similar to macrophage proliferation
393 being a major factor accounting for increased macrophage number during advanced
394 atherosclerosis progression,[47] suppression of proliferation is the predominant mechanism
395 decreasing macrophage burden during regression.[35] Our studies suggest that decreased
396 proliferation of *Jak2*^{VF} macrophages is also a key mechanism decreasing macrophage burden
397 during atherosclerosis regression. Moreover, decreased proliferation was associated with reduced

398 DNA damage response, AIM2 expression and pyroptosis in *Jak2*^{VF} CH lesions, suggesting
399 decreased replication induced DNA damage as the key underlying mechanism responding to
400 cholesterol lowering.

401 Paradoxically, despite the overall reduction in macrophage burden, during regression there may
402 also be a relative increase in a proliferative set of efferocytotic macrophages that also express c-
403 myc expression and contribute to plaque stability.[13,14] However, in addition to a potential role in
404 cell proliferation c-myc has an additional role in Akt signaling and cell survival.[48,49] Previously,
405 we observed a 4-fold increase in TREM2^{Hi} macrophages during atherosclerosis regression
406 induced by both LDL lowering and *Jak2*^{VF} inactivation in *Jak2*^{VF} CH mice.[16] In the present
407 study, we found that LDL lowering alone led to a marked increase in TREM2 staining in
408 macrophages, as well as elevated c-myc expression specifically within TREM2^{Hi} macrophages,
409 in both control and mutant mice. This contrasts with the decreased proliferation and DNA
410 damage response found specifically in the *Jak2*^{VF} macrophages. Our findings together suggest
411 that during regression there is an increase in TREM2^{Hi}, c-myc and MerTK expressing
412 macrophages either through increased proliferation or increased survival of these subsets that
413 then have beneficial effects on efferocytosis and plaque stability. Given that inflammasome
414 activation and IL-1 release have been linked to reduced MerTK and TREM2 as a result of A
415 Disintegrin And Metalloproteinase 17 (ADAM17)-mediated cleavage,[39,50] the increase in this
416 pro-resolving macrophage population may in part be secondary to reduced cholesterol-induced
417 inflammasome activation. Although IL-1β antibodies have been shown to inhibit atherosclerosis
418 regression in *Apoe*$^{-/-}$ mice,[15] IL-1β antibodies improved lesion stability in hypercholesterolemic
419 *Jak2*^{VF} CH mice.[16,29] Elevated IL-1β signaling as a result of increased pyroptosis in *Jak2*^{VF} CH
420 lesions is decreased in the present study as a result of LDL lowering. Combined, these results

421 suggest that excessive IL-1β activation is pro-atherogenic in the context of hypercholesterolemia
422 while a basal level of IL-1β activation may be required for lesion resolution after cholesterol
423 lowering which is blocked when IL-1β antibodies are present.

424 The history of LDL lowering guidelines has been to recommend progressively lower targets
425 based on clinical trial evidence. Current recommendations suggest an LDL cholesterol target
426 below 70 mg/dl for patients with established ACVD or in certain high-risk groups.[51] Statin use
427 has been associated with improved outcomes in human myeloproliferative neoplasm (MPN)
428 patients and was associated with a 37% reduction in the risk of thrombosis in patients who had
429 polycythemia vera or essential thrombocythemia as well as a 22% reduction in all-cause
430 mortality.[52] While data from mice should be extrapolated to humans with caution, the AIM2
431 inflammasome seems to increase ACVD risk in both mice and humans carrying the *Jak2*^{VF}
432 mutation.[30] The present preclinical study adds mechanistic findings to support the idea that
433 aggressive LDL-C lowering in *Jak2*^{VF} MPN patients would reduce ACVD risk.

434 **Acknowledgements**

435 The authors thank Wenli Liu for assistance and support during the course of this study. This
436 study used the Confocal and Specialized Microscopy Shared Resource of the Herbert Irving
437 Comprehensive Cancer Center at Columbia University, funded in part through NIH/NCI Cancer
438 Center Support Grant P30CA013696. Additionally, this study used the resources of the Herbert
439 Irving Comprehensive Cancer Center Flow Cytometry Shared Resources funded in part through
440 Center Grant P30CA013696.

441 **Sources of Funding**

442 This work was supported by grants from the National Institutes of Health and The National
443 Heart, Lung, and Blood Institute: HL155431, HL107653HL170157-02, P01HL172741 to A.R.T
444 and HL148071 to N.W.

445 **Disclosures**

446 A.R.T. is a consultant for CSL Behring and is on the scientific advisory board of Beren
447 Therapeutics. The remaining authors declare no competing financial interests.

448 **Author Contribution Statement**

449 B.H., A.T., N.W., T.F. made substantial contributions to conception, design, data acquisition,
450 analysis, and interpretation. They also drafted and critically reviewed the manuscript for
451 intellectual content. M.T., K.A., C.H., S.S., and T.X. contributed to data acquisition and analysis.

452 **Data Availability Statement**

453 The datasets generated for this study are available from the corresponding author upon
454 reasonable request.

455 **References**

456 1. Martin SS, Aday AW, Almarzooq ZI, Anderson CAM, Arora P, Avery CL, Baker-Smith
457 CM, Barone Gibbs B, Beaton AZ, Boehme AK, Commodore-Mensah Y, Currie ME,
458 Elkind MSV, Evenson KR, Generoso G, Heard DG, Hiremath S, Johansen MC, Kalani R,
459 Kazi DS, Ko D, Liu J, Magnani JW, Michos ED, Mussolino ME, Navaneethan SD,
460 Parikh NI, Perman SM, Poudel R, Rezk-Hanna M, Roth GA, Shah NS, St-Onge MP,
461 Thacker EL, Tsao CW, Urbut SM, Van Spall HGC, Voeks JH, Wang NY, Wong ND,
462 Wong SS, Yaffe K, Palaniappan LP; American Heart Association Council on
463 Epidemiology and Prevention Statistics Committee and Stroke Statistics Subcommittee.
464 2024 Heart Disease and Stroke Statistics: A Report of US and Global Data From the
465 American Heart Association. *Circulation* 2024;**149**:e347–e913.
466 2. Vallejo-Vaz AJ, Fayyad R, Boekholdt SM, Hovingh GK, Kastelein JJP, Melamed S,
467 Barter P, Waters DD, Ray KK. Triglyceride-rich lipoprotein cholesterol and risk of
468 cardiovascular events among patients receiving statin therapy in the TNT trial.
469 *Circulation* 2018;**138**:770–781.
470 3. Cannon CP, Blazing MA, Giugliano RP, McCagg A, White JA, Theroux P, Darius H,
471 Lewis BS, Ophuis TO, Jukema JW, De Ferrari GM, Ruzyllo W, De Lucca P, Im K,
472 Bohula EA, Reist C, Wiviott SD, Tershakovec AM, Musliner TA, Braunwald E, Califf
473 RM; IMPROVE-IT Investigators. Ezetimibe added to statin therapy after acute coronary
474 syndromes. *N Engl J Med* 2015;**372**:2387–2397.
475 4. Sabatine MS, Giugliano RP, Keech AC, Honarpour N, Wiviott SD, Murphy SA, Kuder
476 JF, Wang H, Liu T, Wasserman SM, Sever PS, Pedersen TR; FOURIER Steering

477 Committee and Investigators. Evolocumab and clinical outcomes in patients with
478 cardiovascular disease. *N Engl J Med* 2017;**376**:1713–1722.
479 5. Nidorf SM, Fiolet ATL, Mosterd A, Eikelboom JW, Schut A, Opstal TSJ, The SHK, Xu
480 XF, Ireland MA, Lenderink T, Latchem D, Hoogslag P, Jerzewski A, Nierop P, Whelan A,
481 Hendriks R, Swart H, Schaap J, Kuijper AFM, van Hessen MWJ, Saklani P, Tan I,
482 Thompson AG, Morton A, Judkins C, Bax WA, Dirksen M, Alings M, Hankey GJ,
483 Budgeon CA, Tijssen JGP, Cornel JH, Thompson PL; LoDoCo2 Trial Investigators.
484 Colchicine in patients with chronic coronary disease. *N Engl J Med* 2020;**383**:1838–
485 1847.
486 6. U.S. Food and Drug Administration. Drug approval package: Lodoco (colchicine) tablets,
487 0.5 mg. Approval letter. Published June 16, 2023. Accessed July 5, 2025.
488 https://www.accessdata.fda.gov/drugsatfda_docs/nda/2024/215727Orig1s000Approv.pdf
489 7. Ridker PM, Everett BM, Thuren T, MacFadyen JG, Chang WH, Ballantyne CM, Fonseca
490 F, Nicolau J, Koenig W, Anker SD, Kastelein JJP, Cornel JH, Pais P, Pella D, Genest J,
491 Cifkova R, Lorenzatti A, Forster T, Kobalava Z, Vida-Simiti L, Flather M, Shimokawa H,
492 Ogawa H, Dellborg M, Rossi PRF, Troquay RPT, Libby P, Glynn RJ; CANTOS Trial
493 Group. Antiinflammatory therapy with canakinumab for atherosclerotic disease. *N Engl J*
494 *Med* 2017;**377**:1119–1131.
495 8. Ridker PM. From C-reactive protein to interleukin-6 to interleukin-1: moving upstream to
496 identify novel targets for atheroprotection. *Circ Res* 2016;**118**:145–156.
497 9. Yalcinkaya M, Liu W, Xiao T, Abramowicz S, Wang R, Wang N, Westerterp M, Tall AR.
498 Cholesterol trafficking to the ER leads to the activation of CaMKII/JNK/NLRP3 and
499 promotes atherosclerosis. *J Lipid Res* 2024;**65**:100534.

500 10. Westerterp M, Fotakis P, Ouimet M, Bochem AE, Zhang H, Molusky MM, Wang W,
501 Abramowicz S, la Bastide-van Gemert S, Wang N, Welch CL, Reilly MP, Stroes ES,
502 Moore KJ, Tall AR. Cholesterol efflux pathways suppress inflammasome activation,
503 NETosis, and atherogenesis. *Circulation* 2018;**138**:898–912.
504 11. Yalcinkaya M, Fotakis P, Liu W, Endo-Umeda K, Dou H, Abramowicz S, Xiao T, Libby
505 P, Wang N, Tall AR, Westerterp M. Cholesterol accumulation in macrophages drives
506 NETosis in atherosclerotic plaques via IL-1β secretion. *Cardiovasc Res* 2023;**119**:969–
507 981.
508 12. Sheedy FJ, Grebe A, Rayner KJ, Kalantari P, Ramkhelawon B, Carpenter SB, Becker CE,
509 Ediriweera HN, Mullick AE, Golenbock DT, Stuart LM, Latz E, Fitzgerald KA, Moore
510 KJ. CD36 coordinates NLRP3 inflammasome activation by facilitating intracellular
511 nucleation of soluble ligands into particulate ligands in sterile inflammation. *Nat*
512 *Immunol* 2013;**14**:812–820.
513 13. Gerlach BD, Ampomah PB, Yurdagul A Jr, Liu C, Lauring MC, Wang X, Kasikara C,
514 Kong N, Shi J, Tao W, Tabas I. Efferocytosis induces macrophage proliferation to help
515 resolve tissue injury. *Cell Metab* 2021;**33**:2445–2463.e8.
516 14. Yurdagul A Jr, Subramanian M, Wang X, Crown SB, Ilkayeva OR, Darville L, Kolluru
517 GK, Rymond CC, Gerlach BD, Zheng Z, Kuriakose G, Kevil CG, Koomen JM,
518 Cleveland JL, Muoio DM, Tabas I. Macrophage metabolism of apoptotic cell-derived
519 arginine promotes continual efferocytosis and resolution of injury. *Cell Metab*
520 2020;**31**:518–533.e10.
521 15. Karnewar S, Karnewar V, Deaton RA, Shankman LS, Benavente ED, Williams CM,
522 Bradley X, Alencar GF, Bulut GB, Kirmani S, Baylis RA, Zunder ER, den Ruijter HM,

523 Pasterkamp G, Owens GK. IL-1β inhibition partially negates the beneficial effects of
524 diet-induced atherosclerosis regression in mice. *Arterioscler Thromb Vasc Biol*
525 2024;**44**:1379–1392.
526 16. Fidler TP, Dunbar A, Kim E, Hardaway B, Pauli J, Xue C, Abramowicz S, Xiao T,
527 O'Connor K, Sachs N, Wang N, Maegdefessel L, Levine R, Reilly MP, Tall AR.
528 Suppression of IL-1β promotes beneficial accumulation of fibroblast-like cells in
529 atherosclerotic plaques in clonal hematopoiesis. *Nat Cardiovasc Res* 2024;**3**:60–75.
530 17. Sharma M, Schlegel MP, Afonso MS, Brown EJ, Rahman K, Weinstock A, Sansbury BE,
531 Corr EM, van Solingen C, Koelwyn GJ, Shanley LC, Beckett L, Peled D, Lafaille JJ,
532 Spite M, Loke P, Fisher EA, Moore KJ. Regulatory T cells license macrophage pro-
533 resolving functions during atherosclerosis regression. *Circ Res* 2020;**127**:335–353.
534 18. Zhang X, Rotllan N, Canfrán-Duque A, Sun J, Toczek J, Moshnikova A, Malik S, Price
535 NL, Araldi E, Zhong W, Sadeghi MM, Andreev OA, Bahal R, Reshetnyak YK, Suárez Y,
536 Fernández-Hernando C. Targeted suppression of miRNA-33 using pHLIP improves
537 atherosclerosis regression. *Circ Res* 2022;**131**:77–90.
538 19. Basu D, Hu Y, Huggins LA, Mullick AE, Graham MJ, Wietecha T, Barnhart S, Mogul A,
539 Pfeiffer K, Zirlik A, Fisher EA, Bornfeldt KE, Willecke F, Goldberg IJ. Novel reversible
540 model of atherosclerosis and regression using oligonucleotide regulation of the LDL
541 receptor. *Circ Res* 2018;**122**:560–567.
542 20. Tall AR, Fuster JJ. Clonal hematopoiesis in cardiovascular disease and therapeutic
543 implications. *Nat Cardiovasc Res* 2022;**1**:116–124.
544 21. Jaiswal S, Fontanillas P, Flannick J, Manning A, Grauman PV, Mar BG, Lindsley RC,
545 Mermel CH, Burtt N, Chavez A, Higgins JM, Moltchanov V, Kuo FC, Kluk MJ,

546 Henderson B, Kinnunen L, Koistinen HA, Ladenvall C, Getz G, Correa A, Banahan BF,
547 Gabriel S, Kathiresan S, Stringham HM, McCarthy MI, Boehnke M, Tuomilehto J,
548 Haiman CA, Groop L, Atzmon G, Wilson JG, Neuberg D, Altshuler D, Ebert BL. Age-
549 related clonal hematopoiesis associated with adverse outcomes. *N Engl J Med*
550 2014;**371**:2488–2498.
551 22. Jaiswal S, Natarajan P, Silver AJ, Gibson CJ, Bick AG, Shvartz E, McConkey M, Gupta
552 N, Gabriel S, Ardissino D, Baber U, Mehran R, Fuster V, Danesh J, Frossard P, Saleheen
553 D, Melander O, Sukhova GK, Neuberg D, Libby P, Kathiresan S, Ebert BL. Clonal
554 hematopoiesis and risk of atherosclerotic cardiovascular disease. *N Engl J Med*
555 2017;**377**:111–121.
556 23. Kar SP, Quiros PM, Gu M, Jiang T, Mitchell J, Langdon R, Iyer V, Barcena C,
557 Vijayabaskar MS, Fabre MA, Carter P, Petrovski S, Burgess S, Vassiliou GS. Genome-
558 wide analyses of 200 453 individuals yield new insights into the causes and consequences
559 of clonal hematopoiesis. *Nat Genet* 2022;**54**:1155–1166.
560 24. Bick AG, Weinstock JS, Nandakumar SK, Fulco CP, Bao EL, Zekavat SM, Szeto MD,
561 Liao X, Leventhal MJ, Nasser J, Chang K, Laurie C, Burugula BB, Gibson CJ, Lin AE,
562 Taub MA, Aguet F, Ardlie K, Mitchell BD, Barnes KC, Moscati A, Fornage M, Redline
563 S, Psaty BM, Silverman EK, Weiss ST, Palmer ND, Vasan RS, Burchard EG, Kardia
564 SLR, He J, Kaplan RC, Smith NL, Arnett DK, Schwartz DA, Correa A, de Andrade M,
565 Guo X, Konkle BA, Custer B, Peralta JM, Gui H, Meyers DA, McGarvey ST, Chen IY,
566 Shoemaker MB, Peyser PA, Broome JG, Gogarten SM, Wang FF, Wong Q, Montasser
567 ME, Daya M, Kenny EE, North KE, Launer LJ, Cade BE, Bis JC, Cho MH, Lasky-Su J,
568 Bowden DW, Cupples LA, Mak ACY, Becker LC, Smith JA, Kelly TN, Aslibekyan S,

569 Heckbert SR, Tiwari HK, Yang IV, Heit JA, Lubitz SA, Johnsen JM, Curran JE, Wenzel
570 SE, Weeks DE, Rao DC, Darbar D, Moon JY, Tracy RP, Buth EJ, Rafaels N, Loos RJF,
571 Durda P, Liu Y, Hou L, Lee J, Kachroo P, Freedman BI, Levy D, Bielak LF, Hixson JE,
572 Floyd JS, Whitsel EA, Ellinor PT, Irvin MR, Fingerlin TE, Raffield LM, Armasu SM,
573 Wheeler MM, Sabino EC, Blangero J, Williams LK, Levy BD, Sheu WH, Roden DM,
574 Boerwinkle E, Manson JE, Mathias RA, Desai P, Taylor KD, Johnson AD; NHLBI Trans-
575 Omics for Precision Medicine Consortium; Auer PL, Kooperberg C, Laurie CC,
576 Blackwell TW, Smith AV, Zhao H, Lange E, Lange L, Rich SS, Rotter JI, Wilson JG,
577 Scheet P, Kitzman JO, Lander ES, Engreitz JM, Ebert BL, Reiner AP, Jaiswal S, Abecasis
578 G, Sankaran VG, Kathiresan S, Natarajan P. Inherited causes of clonal haematopoiesis in
579 97,691 whole genomes. *Nature* 2020;**586**:763–768.
580 25. Cordua S, Kjaer L, Skov V, Pallisgaard N, Hasselbalch HC, Ellervik C. Prevalence and
581 phenotypes of JAK2 V617F and calreticulin mutations in a Danish general population.
582 *Blood* 2019;**134**:469–479.
583 26. Wang S, Luo X, Hu S, Zhao C, Sun Q, Zeng M, Bao X, Wang Y, Wu F, Yang Y, Lv Y, Bai
584 X, Hao W, Liu M, Yi B, Chen Y, Meng W, Li J, Li M, Huang J, Wu T, Zhao Y, Zhang Z,
585 An J, Libby P, Jia H, Yu B. Plaque erosion risk and JAK2 V617F variant. *Eur Heart J*
586 2025;**46**:2205–2219.
587 27. Molinaro R, Sellar RS, Vromman A, Sausen G, Folco E, Sukhova GK, McConke ME,
588 Corbo C, Ebert BL, Libby P. The clonal hematopoiesis mutation Jak2V617F aggravates
589 endothelial injury and thrombosis in arteries with erosion-like intimas. *Int J Cardiol*
590 2024;**409**:132184.

591 28. Liu W, Pircher J, Schuermans A, Ul Ain Q, Zhang Z, Honigberg MC, Yalcinkaya M,
592 Nakao T, Pournamadri A, Xiao T, Hajebrahimi MA, Wasner L, Stegner D, Petzold T,
593 Natarajan P, Massberg S, Tall AR, Schulz C, Wang N. Jak2 V617F clonal hematopoiesis
594 promotes arterial thrombosis via platelet activation and cross talk. *Blood* 2024;**143**:1539–
595 1550.
596 29. Fidler TP, Xue C, Yalcinkaya M, Hardaway B, Abramowicz S, Xiao T, Liu W, Thomas
597 DG, Hajebrahimi MA, Pircher J, Silvestre-Roig C, Kotini AG, Luchsinger LL, Wei Y,
598 Westerterp M, Snoeck HW, Papapetrou EP, Schulz C, Massberg S, Soehnlein O, Ebert
599 BL, Levine RL, Reilly MP, Libby P, Wang N, Tall AR. The AIM2 inflammasome
600 exacerbates atherosclerosis in clonal haematopoiesis. *Nature* 2021;**592**:296–301.
601 30. Yu Z, Fidler TP, Ruan Y, Vlasschaert C, Nakao T, Uddin MM, Mack T, Niroula A,
602 Heimlich JB, Zekavat SM, Gibson CJ, Griffin GK, Wang Y, Peloso GM, Heard-Costa N,
603 Levy D, Vasan RS, Aguet F, Ardlie KG, Taylor KD, Rich SS, Rotter JI, Libby P, Jaiswal
604 S, Ebert BL, Bick AG, Tall AR, Natarajan P. Genetic modification of inflammation- and
605 clonal hematopoiesis-associated cardiovascular risk. *J Clin Invest* 2023;**133**:e168597.
606 31. Rathinam VA, Fitzgerald KA. Inflammasome complexes: emerging mechanisms and
607 effector functions. *Cell* 2016;**165**:792–800.
608 32. Mullally A, Lane SW, Ball B, Megerdichian C, Okabe R, Al-Shahrour F, Paktinat M,
609 Haydu JE, Housman E, Lord AM, Wernig G, Kharas MG, Mercher T, Kutok JL, Gilliland
610 DG, Ebert BL. Physiological Jak2V617F expression causes a lethal myeloproliferative
611 neoplasm with differential effects on hematopoietic stem and progenitor cells. *Cancer*
612 *Cell* 2010;**17**:584–596.

613 33. Pan H, Xue C, Auerbach BJ, Fan J, Bashore AC, Cui J, Yang DY, Trignano SB, Liu W,
614 Shi J, Ihuegbu CO, Bush EC, Worley J, Vlahos L, Laise P, Solomon RA, Connolly ES,
615 Califano A, Sims PA, Zhang H, Li M, Reilly MP. Single-cell genomics reveals a novel
616 cell state during smooth muscle cell phenotypic switching and potential therapeutic
617 targets for atherosclerosis in mouse and human. *Circulation* 2020;**142**:2060–2075.
618 34. Kar SP, Quiros PM, Gu M, Jiang T, Mitchell J, Langdon R, Iyer V, Barcena C,
619 Vijayabaskar MS, Fabre MA, Carter P, Petrovski S, Burgess S, Vassiliou GS. Genome-
620 wide analyses of 200 453 individuals yield new insights into the causes and consequences
621 of clonal hematopoiesis. *Nat Genet* 2022;**54**:1155–1166.
622 35. Härdtner C, Kornemann J, Krebs K, Ehlert CA, Jander A, Zou J, Starz C, Rauterberg S,
623 Sharipova D, Dufner B, Hoppe N, Dederichs TS, Willecke F, Stachon P, Heidt T, Wolf D,
624 von Zur Mühlen C, Madl J, Kohl P, Kaeser R, Boettler T, Pieterman EJ, Princen HMG,
625 Ho-Tin-Noé B, Swirski FK, Robbins CS, Bode C, Zirlik A, Hilgendorf I. Inhibition of
626 macrophage proliferation dominates plaque regression in response to cholesterol
627 lowering. *Basic Res Cardiol* 2020;**115**:78.
628 36. Peled M, Nishi H, Weinstock A, Barrett TJ, Zhou F, Quezada A, Fisher EA. A wild-type
629 mouse-based model for the regression of inflammation in atherosclerosis. *PLoS One*
630 2017;**12**:e0173975.
631 37. Broz P. Pyroptosis: molecular mechanisms and roles in disease. *Cell Res* 2025;**35**:334–
632 344.
633 38. Liu W, Hardaway BD, Kim E, Pauli J, Wettich JL, Yalcinkaya M, Hsu CC, Xiao T, Reilly
634 MP, Tabas I, Maegdefessel L, Schlepckow K, Haass C, Wang N, Tall AR. Inflammatory

635 crosstalk impairs phagocytic receptors and aggravates atherosclerosis in clonal
636 hematopoiesis in mice. *J Clin Invest* 2024;**135**:e182939.
637 39. Ngai D, Schilperoort M, Tabas I. Efferocytosis-induced lactate enables the proliferation
638 of pro-resolving macrophages to mediate tissue repair. *Nat Metab* 2023;**5**:2206–2219.
639 40. Sukka SR, Ampomah PB, Darville LNF, Ngai D, Wang X, Kuriakose G, Xiao Y, Shi J,
640 Koomen JM, McCusker RH, Tabas I. Efferocytosis drives a tryptophan metabolism
641 pathway in macrophages to promote tissue resolution. *Nat Metab* 2024;**6**:1736–1755.
642 41. Patterson MT, Xu Y, Hillman H, Osinski V, Schrank PR, Kennedy AE, Barrow F, Zhu A,
643 Tollison S, Shekhar S, Stromnes IM, Tassi I, Wu D, Revelo XS, Binstadt BA, Williams
644 JW. Trem2 agonist reprograms foamy macrophages to promote atherosclerotic plaque
645 stability — brief report. *Arterioscler Thromb Vasc Biol* 2024;**44**:1646–1657.
646 42. Corsini A, Mazzotti M, Villa A, Maggi FM, Bernini F, Romano L, Romano C, Fumagalli
647 R, Catapano AL. Ability of the LDL receptor from several animal species to recognize
648 the human apo B binding domain: studies with LDL from familial defective apo B-100.
649 *Atherosclerosis* 1992;**93**:95–103.
650 43. Innerarity TL, Pitas RE, Mahley RW. Disparities in the interaction of rat and human
651 lipoproteins with cultured rat fibroblasts and smooth muscle cells: requirements for
652 homology for receptor binding activity. *J Biol Chem* 1980;**255**:11163–11172.
653 44. Lin JD, Nishi H, Poles J, Niu X, McCauley C, Rahman K, Brown EJ, Yeung ST, Vozhilla
654 N, Weinstock A, Ramsey SA, Fisher EA, Loke P. Single-cell analysis of fate-mapped
655 macrophages reveals heterogeneity, including stem-like properties, during atherosclerosis
656 progression and regression. *JCI Insight* 2019;**4**:e124574.

657 45. Feig JE, Pineda-Torra I, Sanson M, Bradley MN, Vengrenyuk Y, Bogunovic D, Gautier
658 EL, Rubinstein D, Hong C, Liu J, Wu C, van Rooijen N, Bhardwaj N, Garabedian M,
659 Tontonoz P, Fisher EA. LXR promotes the maximal egress of monocyte-derived cells
660 from mouse aortic plaques during atherosclerosis regression. *J Clin Invest*
661 2010;**120**:4415–4424.
662 46. Nagareddy PR, Murphy AJ, Stirzaker RA, Hu Y, Yu S, Miller RG, Ramkhelawon B,
663 Distel E, Westerterp M, Huang LS, Schmidt AM, Orchard TJ, Fisher EA, Tall AR,
664 Goldberg IJ. Hyperglycaemia promotes myelopoiesis and impairs the resolution of
665 atherosclerosis. *Cell Metab* 2013;**17**:695–708.
666 47. Robbins CS, Hilgendorf I, Weber GF, Theurl I, Iwamoto Y, Figueiredo JL, Gorbatov R,
667 Sukhova GK, Gerhardt LM, Smyth D, Zavitz CC, Shikatani EA, Parsons M, van Rooijen
668 N, Lin HY, Husain M, Libby P, Nahrendorf M, Weissleder R, Swirski FK. Local
669 proliferation dominates lesional macrophage accumulation in atherosclerosis. *Nat Med*
670 2013;**19**:1166–1172.
671 48. Miller DM, Thomas SD, Islam A, Muench D, Sedoris K. c-Myc and cancer metabolism.
672 *Clin Cancer Res* 2012;**18**:5546–5553.
673 49. Wise DR, DeBerardinis RJ, Mancuso A, Sayed N, Zhang XY, Pfeiffer HK, Nissim I,
674 Daikhin E, Yudkoff M, McMahon SB, Thompson CB. Myc regulates a transcriptional
675 program that stimulates mitochondrial glutaminolysis and leads to glutamine addiction.
676 *Proc Natl Acad Sci U S A* 2008;**105**:18782–18787.
677 50. Endo-Umeda K, Kim E, Thomas DG, Liu W, Dou H, Yalcinkaya M, Abramowicz S, Xiao
678 T, Antonson P, Gustafsson JÅ, Makishima M, Reilly MP, Wang N, Tall AR. Myeloid
679 LXR (liver X receptor) deficiency induces inflammatory gene expression in foamy

680 macrophages and accelerates atherosclerosis. *Arterioscler Thromb Vasc Biol*
681 2022;**42**:719–731.
682 51. Virani SS, Newby LK, Arnold SV, Bittner V, Brewer LC, Demeter SH, Dixon DL, Fearon
683 WF, Hess B, Johnson HM, Kazi DS, Kolte D, Kumbhani DJ, LoFaso J, Mahtta D, Mark
684 DB, Minissian M, Navar AM, Patel AR, Piano MR, Rodriguez F, Talbot AW, Taqueti VR,
685 Thomas RJ, van Diepen S, Wiggins B, Williams MS; Peer Review Committee Members.
686 2023 AHA/ACC/ACCP/ASPC/NLA/PCNA guideline for the management of patients
687 with chronic coronary disease: a report of the American Heart Association/American
688 College of Cardiology Joint Committee on Clinical Practice Guidelines. *Circulation*
689 2023;**148**:e9–e119.
690 52. Podoltsev NA, Wang R, Shallis RM, Stempel JM, Di M, Neparidze N, Zeidan AM,
691 Huntington SF, Giri S, Hull SC, Gore SD, Ma X. Statin use, survival and incidence of
692 thrombosis among older patients with polycythemia vera and essential thrombocythemia.
693 *Cancer Med* 2023;**12**:18889–18900.

694

Figure 1

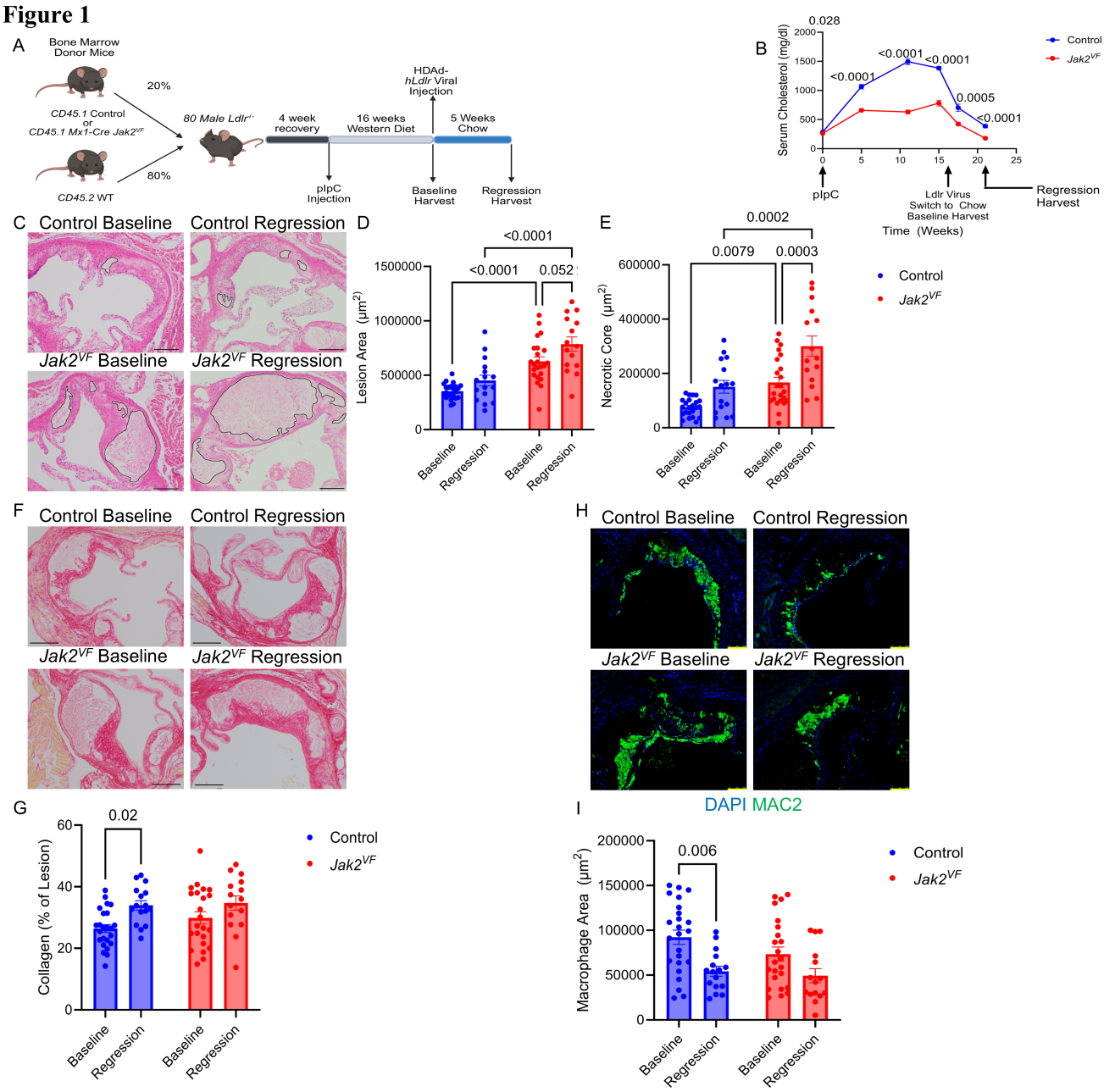
A
Bone Marrow Donor Mice
CD45.1 Control or CD45.1 Mx1-Cre Jak2VF
CD45.2 WT
20%
80%
80 Male Ldlr-/-
4 week recovery
16 weeks Western Diet
HDAd-hLdlr Viral Injection
5 Weeks Chow
pIpC Injection
Baseline Harvest
Regression Harvest
B
Serum Cholesterol (mg/dl)
Time (Weeks)
Control
Jak2VF
pIpC
Ldlr Virus Switch to Chow Baseline Harvest
Regression Harvest
C
Control Baseline
Control Regression
Jak2VF Baseline
Jak2VF Regression
D
Lesion Area (μm2)
E
Necrotic Core (μm2)
F
G
Collagen (% of Lesion)
H
DAPI MAC2
I
Macrophage Area (μm2)
Baseline
Regression

695 **Figure 1. Impaired Atherosclerosis Regression in *Jak2^{VF}* CH Mice with Moderate**
696 **Cholesterol Lowering. A.** Study Design. **B.** Plasma cholesterol (n = 34, 55, 55, 54, 16, 16 for
697 Control mice, n=31, 55, 49, 39, 17, 16 for *Jak2^{VF}* mice, for weeks 0, 5, 11, 15, 17.5, 21
698 respectively). **C.** H&E images of aortic root lesions. Black lines, necrotic core. Scale bar, 200
699 µm. **D.** Lesion area, n = 15-23. **E.** Necrotic core area, n = 15-23. **F.** Picrosirius red-stained aortic
700 root lesions. Scale bar, 278 µm **G.** Collagen area as a percentage of lesion area, n = 15-24. **H.**
701 Images of aortic root lesions stained for MAC2 (Green) and DAPI (Blue). Scale bar, 100 µm. **I.**
702 Macrophage area, n = 15-24. All quantifications shown as mean ± s.e.m. Two-way ANOVA with
703 the Geisser-Greenhouse correction for sphericity and Tukey's multiple comparisons test (B).
704 Two-way ANOVA with Tukey's multiple comparisons test (D,E,G,I).

705 **Figure 2**

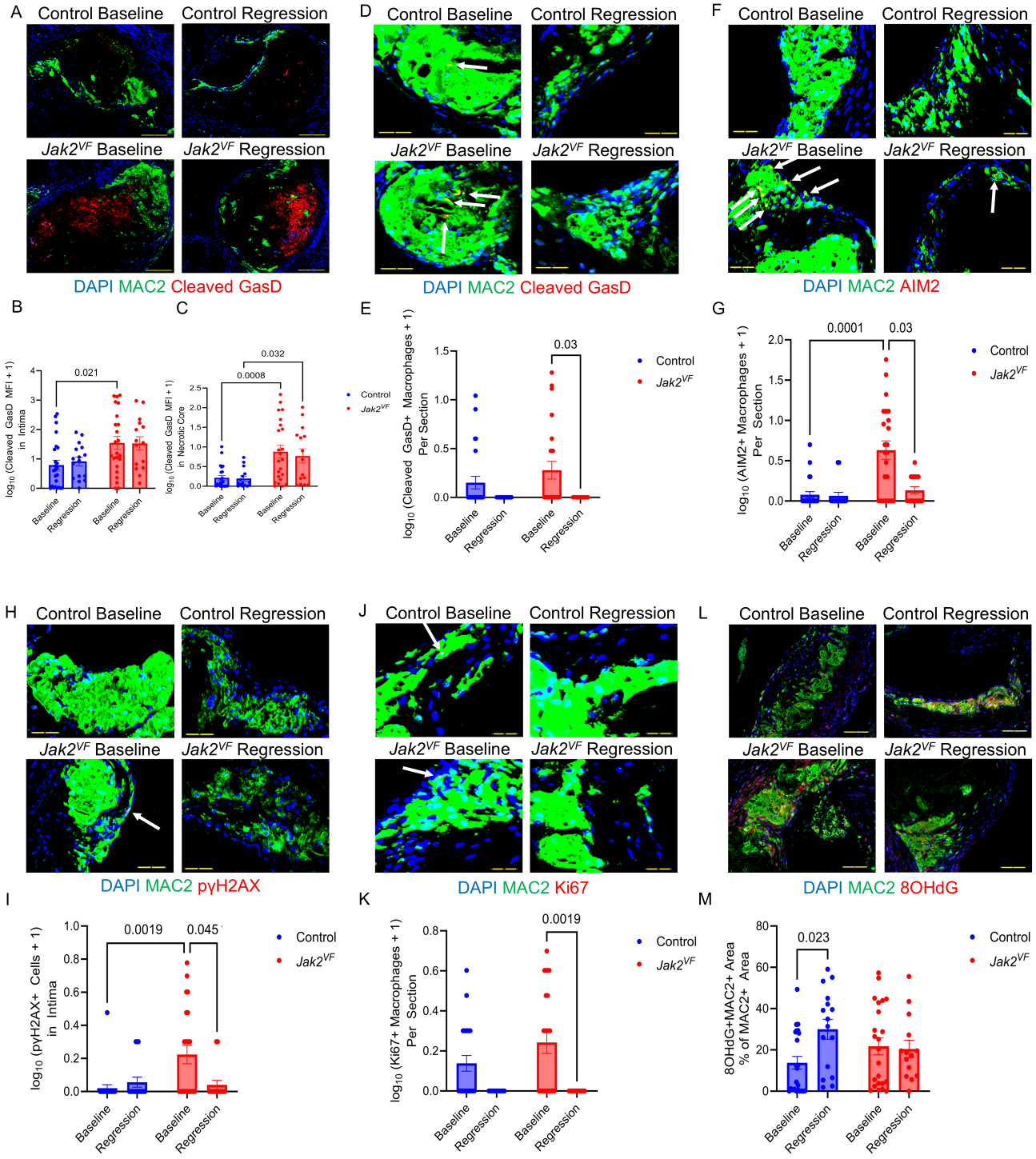
A
Control Baseline
Control Regression
Jak2VF Baseline
Jak2VF Regression
DAPI MAC2 Cleaved GasD
B
log10 (Cleaved GasD MFI + 1) in Intima
0.021
Baseline
Regression
C
log10 (Cleaved GasD MFI + 1) in Necrotic Core
0.0008
0.032
D
E
log10 (Cleaved GasD+ Macrophages + 1) Per Section
0.03
Control
Jak2VF
F
DAPI MAC2 AIM2
G
log10 (AIM2+ Macrophages + 1) Per Section
0.0001
0.03
H
DAPI MAC2 pγH2AX
I
log10 (pγH2AX+ Cells + 1) in Intima
0.0019
0.045
J
DAPI MAC2 Ki67
K
log10 (Ki67+ Macrophages + 1) Per Section
0.0019
L
DAPI MAC2 8OHdG
M
8OHdG+MAC2+ Area % of MAC2+ Area
0.023

706 **Figure 2. Moderate Cholesterol Lowering Reverses Macrophage AIM2 Inflammasome**
707 **Activation, DNA Damage, and Proliferation in *Jak2*^{VF} CH Lesions. A.** Images of aortic root
708 lesions stained for MAC2 (Green), Cleaved GasD (Red), and DAPI (Blue). Scale bar, 127 µm. **B.**
709 Log_{10} transformed cleaved GasD mean fluorescence intensity (MFI) in lesions with the addition
710 of constant 1, n = 15-24. **C.** Log_{10} transformed cleaved GasD mean fluorescence intensity (MFI)
711 in necrotic cores with the addition of the constant 1, n = 15-24. **D.** Images of aortic root lesions
712 stained for MAC2 (Green), Cleaved GasD (Red), and DAPI (Blue). Scale bar, 40 µm. White
713 arrows, cleaved GasD+ macrophages. **E.** Log_{10} transformed cleaved GasD positive macrophages
714 per section with the addition of constant 1, n = 15-24. **F.** Images of aortic root lesions stained for
715 MAC2 (Green), AIM2 (Red), and DAPI (Blue). Scale bar, 75 µm. White arrows, AIM2 positive
716 macrophages. **G.** Log_{10} transformed AIM2 positive macrophages per section with the addition of
717 constant 1, n = 15-23. **H.** Images of aortic root lesions stained for MAC2 (Green), pγH2AX
718 (Red), and DAPI (Blue). Scale bar, 46 µm. White arrows, pγH2AX positive cells. **I.** Log_{10}
719 transformed pγH2AX positive macrophages per section with the addition of constant 1, n = 15-
720 23. **J.** Images of aortic root lesions stained for MAC2 (Green), Ki67 (Red), and DAPI (Blue).
721 Scale bar, 25 µm. White arrows, Ki67 positive macrophages. **K.** Log_{10} transformed Ki67 positive
722 macrophages per section with the addition of constant 1, n = 15-23. **L.** Images of aortic root
723 lesions stained for MAC2 (Green), 8OHdG (Red), and DAPI (Blue). Scale bar, 78 µm. **M.**
724 Percentage of MAC2 positive area double positive for 8OHdG and MAC2, n = 14-24. MAC2
725 intensity differences reflect independent staining and imaging sessions across panels. All
726 quantifications shown as mean ± s.e.m. Two-way ANOVA with Tukey's multiple comparisons
727 test (B,C). Kruskal-Wallis test with Dunn's multiple comparisons test (E,G,I,K,M).

728 **Figure 3**

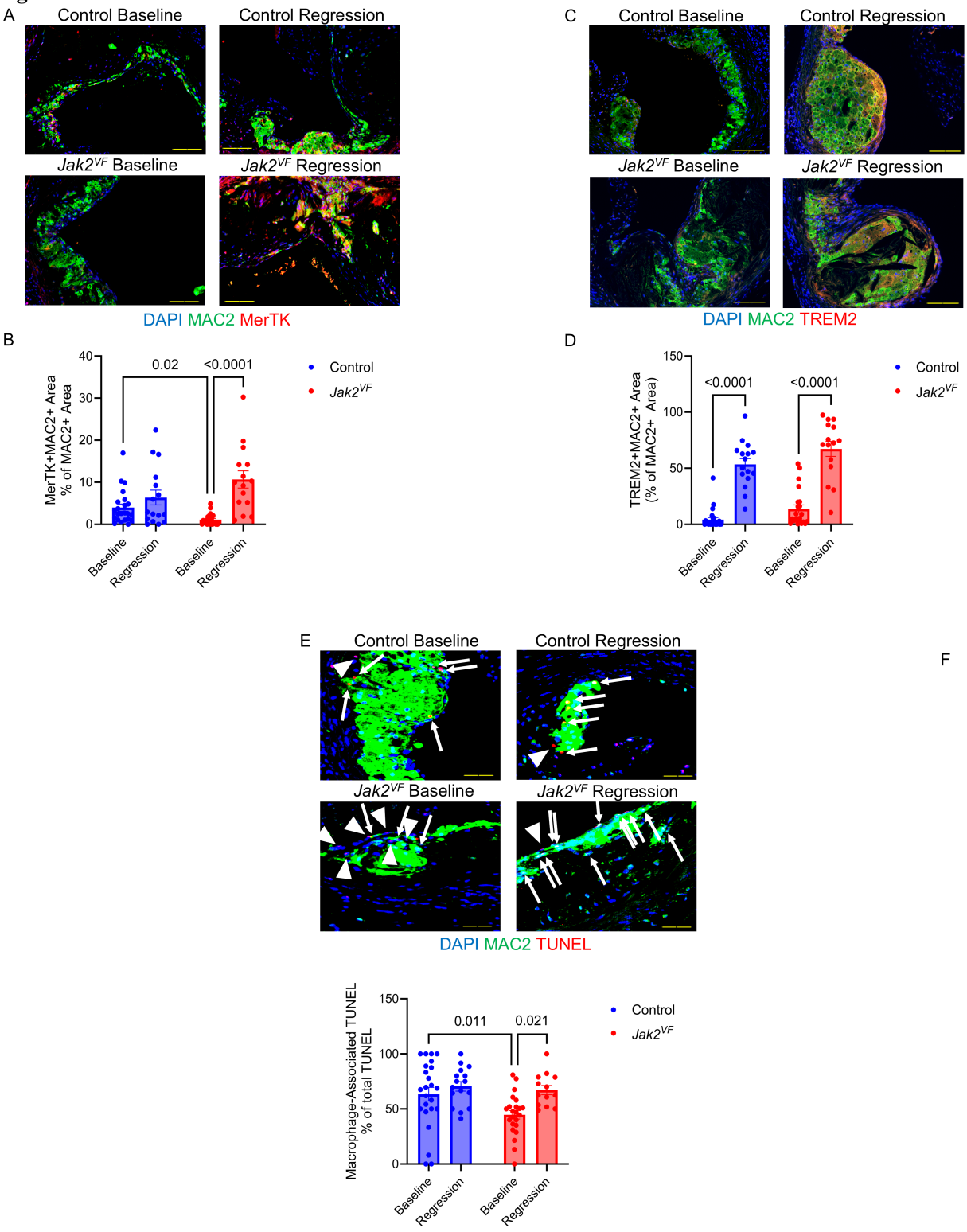
A
Control Baseline
Control Regression
Jak2VF Baseline
Jak2VF Regression
DAPI MAC2 MerTK
B
MerTK+MAC2+ Area
% of MAC2+ Area
0.02
<0.0001
Control
Jak2VF
Baseline
Regression
Baseline
Regression
C
Control Baseline
Control Regression
Jak2VF Baseline
Jak2VF Regression
DAPI MAC2 TREM2
D
TREM2+MAC2+ Area
(% of MAC2+ Area)
<0.0001
<0.0001
Control
Jak2VF
Baseline
Regression
Baseline
Regression
E
Control Baseline
Control Regression
Jak2VF Baseline
Jak2VF Regression
DAPI MAC2 TUNEL
F
Macrophage-Associated TUNEL
% of total TUNEL
0.011
0.021
Control
Jak2VF
Baseline
Regression
Baseline
Regression

729 **Figure 3. Moderate Cholesterol Lowering Reverses Impaired Efferocytosis in *Jak2*^{VF} CH**
730 **Lesions While Increasing TREM2^{Hi} Macrophages in Control and *Jak2*^{VF} CH Lesions A.**
731 Images of aortic root lesions stained for MAC2 (Green), MerTK (Red), and DAPI (Blue). Scale
732 bar, 102 µm. **B.** Percentage of MAC2 positive area double positive for MerTK and MAC2, n =
733 15-23. **C.** Images of aortic root lesions stained for MAC2 (Green), TREM2 (Red), and DAPI
734 (Blue). Scale bar, 100 µm. **D.** Percentage of MAC2 positive area double positive for TREM2 and
735 MAC2, n = 15-24. **E.** Images of in situ efferocytosis in aortic root lesions: MAC2 (Green),
736 TUNEL (Red), and DAPI (Blue). Scale bar, 40 µm. White arrows, nuclei double positive for
737 TUNEL and MAC2. White wedges, nuclei positive for TUNEL but negative for MAC2. **F.**
738 Percentage of TUNEL positive nuclei also positive for MAC2. MAC2 intensity differences
739 reflect independent staining and imaging sessions across panels, n = 13-24. All quantifications
740 shown as mean ± s.e.m. Two-way ANOVA with Tukey's multiple comparisons test (D). Kruskal-
741 Wallis test with Dunn's multiple comparisons test (B,F).

742

Figure 4

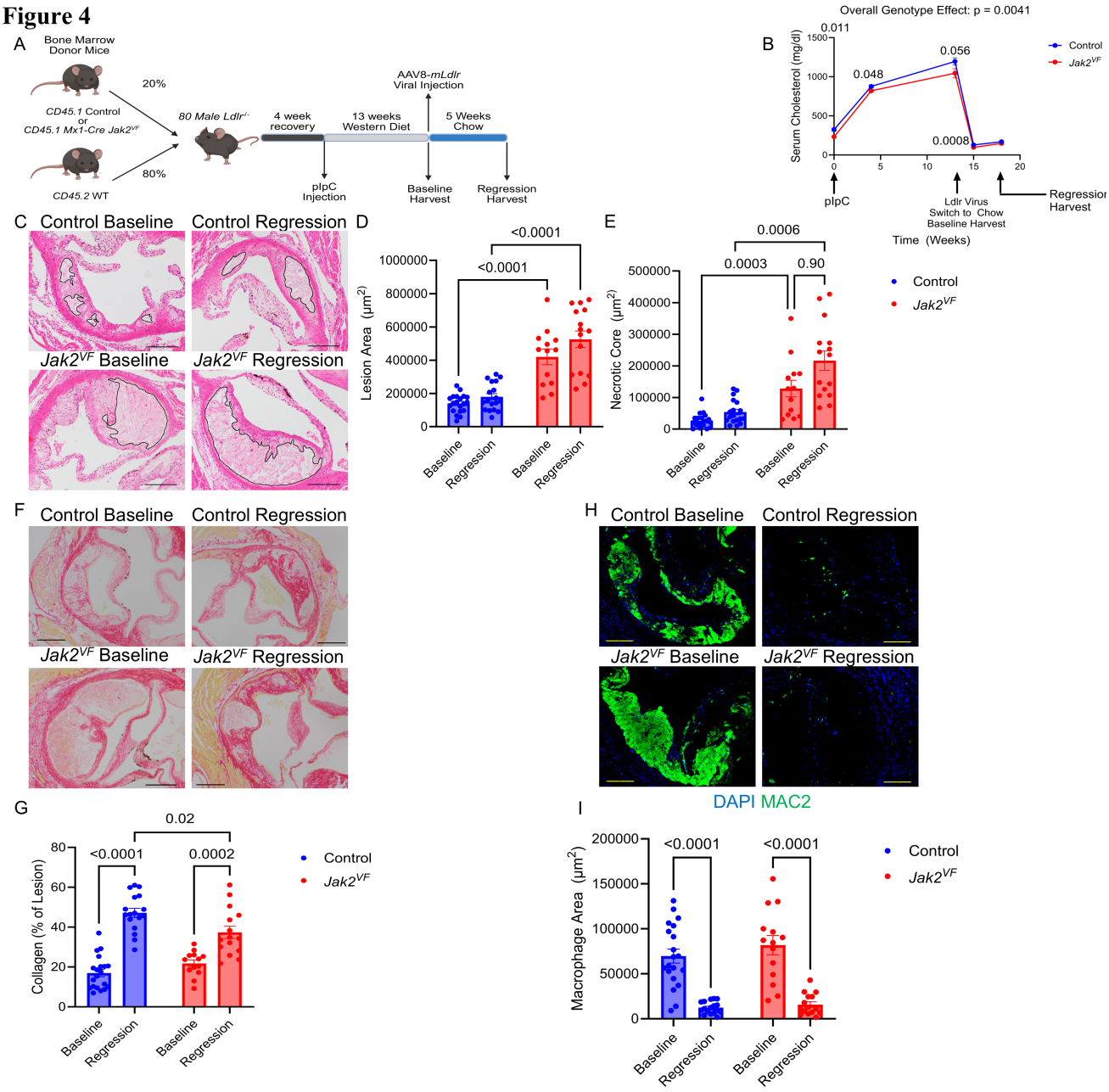
A
Bone Marrow Donor Mice
20%
80%
CD45.1 Control or CD45.1 Mx1-Cre Jak2VF
CD45.2 WT
80 Male Ldlr-/-
4 week recovery
13 weeks Western Diet
AAV8-mLdlr Viral Injection
5 Weeks Chow
pIpC Injection
Baseline Harvest
Regression Harvest
B
Overall Genotype Effect: p = 0.0041
Serum Cholesterol (mg/dl)
0.011
0.048
0.056
0.0008
Control
Jak2VF
pIpC
Ldlr Virus Switch to Chow Baseline Harvest
Regression Harvest
Time (Weeks)
C
Control Baseline
Control Regression
Jak2VF Baseline
Jak2VF Regression
D
Lesion Area (μm2)
<0.0001
<0.0001
Baseline
Regression
E
Necrotic Core (μm2)
0.0006
0.0003
0.90
Control
Jak2VF
F
Control Baseline
Control Regression
Jak2VF Baseline
Jak2VF Regression
H
Control Baseline
Control Regression
Jak2VF Baseline
Jak2VF Regression
DAPI MAC2
G
Collagen (% of Lesion)
0.02
<0.0001
0.0002
Control
Jak2VF
I
Macrophage Area (μm2)
<0.0001
<0.0001
Control
Jak2VF

743 **Figure 4. Aggressive Cholesterol Lowering Normalizes Regression in *Jak2^{VF}* CH Lesions. A.**
744 Study Design. **B.** Plasma cholesterol (n = 5, 38, 19, 18, 18 for Control mice, n = 5, 37, 15, 16, 15
745 for Jak2VF mice, for weeks 0, 4, 13, 15, 18 respectively). **C.** H&E images of aortic root lesions.
746 Black lines, necrotic core. Scale bar, 200 µm. **D.** Lesion area, n = 13-20. **E.** Necrotic core area, n
747 = 13-20. **F.** Picrosirius red-stained aortic root lesions. Scale bar, 219 µm **G.** Collagen area as a
748 percentage of lesion area, n = 13-20. **H.** Images of aortic root lesions stained for MAC2 (Green)
749 and DAPI (Blue). Scale bar, 193 µm. **I.** Macrophage area, n = 13-20. All quantifications shown
750 as mean ± s.e.m. Two-way ANOVA with Tukey's multiple comparisons test (D,G,I). Two-way
751 ANOVA with the Geisser-Greenhouse correction for sphericity and Tukey's multiple
752 comparisons test (B). Kruskal-Wallis test with Dunn's multiple comparisons test (E)

753 **Figure 5**

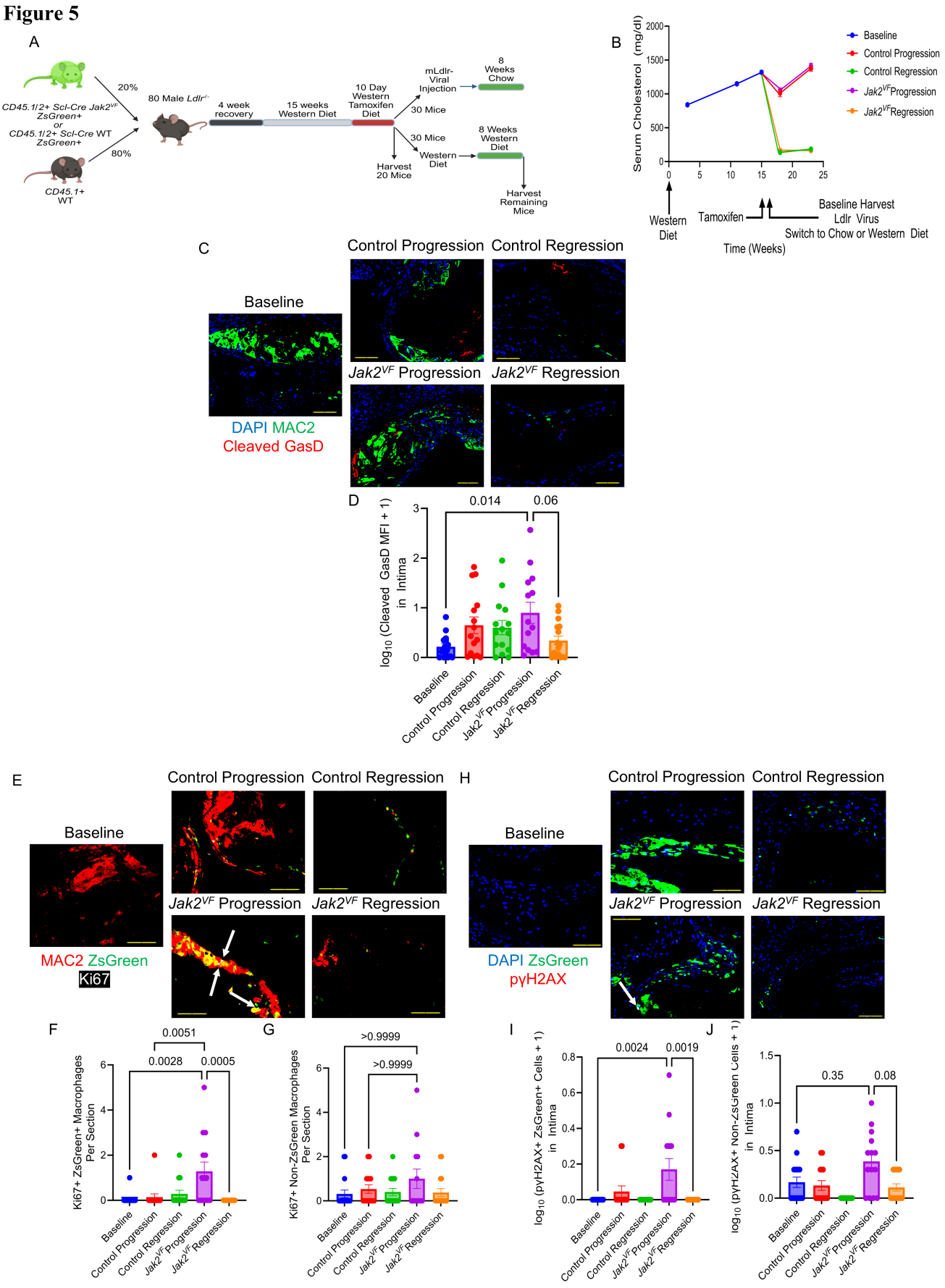
A
CD45.1/2+ Scl-Cre Jak2VF ZsGreen+
or
CD45.1/2+ Scl-Cre WT ZsGreen+
20%
80%
CD45.1+ WT
80 Male Ldlr-/-
4 week recovery
15 weeks Western Diet
10 Day Western Tamoxifen Diet
mLdlr-Viral Injection
8 Weeks Chow
30 Mice
30 Mice
Harvest 20 Mice
Western Diet
8 Weeks Western Diet
Harvest Remaining Mice
B
Serum Cholesterol (mg/dl)
Baseline
Control Progression
Control Regression
Jak2VFProgression
Jak2VFRegression
Western Diet
Tamoxifen
Baseline Harvest
Ldlr Virus
Switch to Chow or Western Diet
Time (Weeks)
C
Baseline
Control Progression
Control Regression
Jak2VF Progression
Jak2VF Regression
DAPI MAC2
Cleaved GasD
D
log10 (Cleaved GasD MFI + 1) in Intima
0.014
0.06
Baseline
Control Progression
Control Regression
Jak2VF Progression
Jak2VF Regression
E
Baseline
Control Progression
Control Regression
Jak2VF Progression
Jak2VF Regression
MAC2 ZsGreen
Ki67
F
Ki67+ ZsGreen+ Macrophages Per Section
0.0051
0.0028
0.0005
G
Ki67+ Non-ZsGreen Macrophages Per Section
>0.9999
>0.9999
H
Baseline
Control Progression
Control Regression
Jak2VF Progression
Jak2VF Regression
DAPI ZsGreen
pγH2AX
I
log10 (pγH2AX+ ZsGreen+ Cells + 1) in Intima
0.0024
0.0019
J
log10 (pγH2AX+ Non-ZsGreen Cells + 1) in Intima
0.35
0.08

754 **Figure 5. Cholesterol Lowering Suppresses *Jak2^{VF}* Macrophage Proliferation and DNA**
755 **Damage. A.** Study design. **B.** Plasma cholesterol (n = 80, 79, 79 for Baseline mice for weeks 3,
756 11, 15 respectively; n = 13, 15 for Control Progression mice, n = 16, 16 for Control Regression
757 mice, n = 15, 15 for *Jak2^{VF}* Progression mice, n = 16, 16 for *Jak2^{VF}* Regression mice, for weeks
758 18, 23 respectively) **C.** Images of aortic root lesions for MAC2 (Green), Cleaved GasD (Red),
759 and DAPI (Blue). Scale bar, 98 µm. **D.** Log_{10} transformed cleaved GasD mean fluorescence
760 intensity (MFI) in lesions with the addition of constant 1, n = 14-16. **E.** Images of aortic root
761 lesions for MAC2 (Red), Ki67 (White), and ZsGreen (Green). Scale bar, 133 µm. White arrows,
762 macrophages double positive for Ki67 and ZsGreen. **F.** Macrophages positive for both Ki67 and
763 ZsGreen per section, n = 14-15. **G.** Macrophages positive for Ki67 but negative for ZsGreen per
764 section, n = 13-16. **H.** Images of aortic root lesions stained for pγH2AX (Red), ZsGreen (Green),
765 and DAPI (Blue). Scale bar, 75 µm. White arrows, pγH2AX positive cells. **I.** Log_{10} transformed
766 cells double positive for pγH2AX and ZsGreen in lesions with the addition of constant 1, n = 13-
767 16. **J.** Log_{10} transformed cells positive for pγH2AX but negative for ZsGreen in lesions with the
768 addition of constant 1, n = 13-16. All quantifications shown as mean ± s.e.m. One-way ANOVA
769 with Holm-Sidak's multiple comparisons test (D). Kruskal-Wallis test with Dunn's multiple
770 comparison's test (F,G,I,J).

771 **Figure 6**

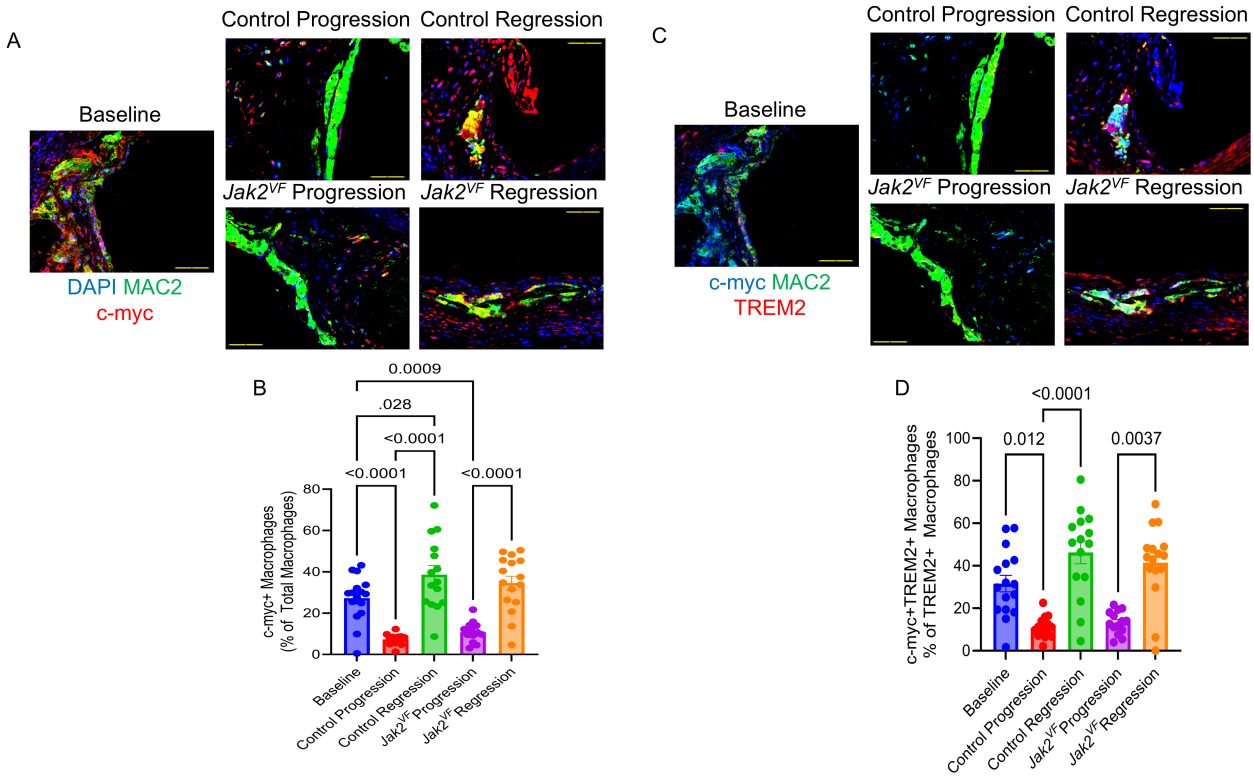
A
Baseline
Control Progression
Control Regression
Jak2VF Progression
Jak2VF Regression
DAPI MAC2
c-myc
B
c-myc+ Macrophages
(% of Total Macrophages)
0.0009
.028
<0.0001
<0.0001
<0.0001
Baseline
Control Progression
Control Regression
Jak2VF Progression
Jak2VF Regression
C
Baseline
Control Progression
Control Regression
Jak2VF Progression
Jak2VF Regression
c-myc MAC2
TREM2
D
c-myc+TREM2+ Macrophages
% of TREM2+ Macrophages
<0.0001
0.012
0.0037
Baseline
Control Progression
Control Regression
Jak2VF Progression
Jak2VF Regression

772 **Figure 6. Cholesterol Lowering Increases c-myc in TREM2^{Hi} Macrophages. A.** Images of
773 aortic root lesions stained for MAC2 (Green), c-myc (Red), and DAPI (Blue). Scale bar, 121 µm.
774 **B.** Percentage of macrophages positive for c-myc, n = 14-16. **C.** Images of aortic root lesions
775 stained for MAC2 (Green), c-myc (Blue), and TREM2 (Red). Scale bar, 121 µm. **D.** Percentage
776 of TREM2 positive macrophages positive for c-myc, n = 14-16. All quantifications shown as
777 mean ± s.e.m. One-way ANOVA with Holm-Sidak's multiple comparisons test (B). Kruskal-
778 Wallis test with Dunn's multiple comparisons test (D).